Supporting Online Material for

Engineering Entropy-Driven Reactions and Networks Catalyzed by DNA

David Yu Zhang,* Andrew J. Turberfield, Bernard Yurke, Erik Winfree*

*To whom correspondence should be addressed. E-mail: winfree@caltech.edu (E.W.); dzhang@dna.caltech.edu (D.Y.Z.)

Published 16 November 2007, *Science* **318**, 1121 (2007)

DOI: 10.1126/science.1148532

This PDF file includes:

Engineering Entropy-Driven Reactions and Networks Catalyzed by DNA

Supplemental Materials

David Y Zhang,[1] Andrew J Turberfield,[2] Bernard Yurke,[3] and Erik Winfree[1]

[1] *California Institute of Technology, MC 136-93, 1200 E. California Blvd., Pasadena, CA 91125*
[2] *University of Oxford, Clarendon Laboratory, Parks Road, Oxford OX1 3PU, United Kingdom*
[3] *Bell Laboratories, Alcatel-Lucent, Murray Hill, NJ 07974*

S1. DNA sequence design

The DNA sequence design process was done on a domain level. Domains denoted by unmodified numbers are termed primary domains, while domains denoted by barred numbers are termed complementary domains. First, random sequences composed of only A, C, and T were generated for each of the primary domains. Since in the intended reaction pathway only primary domains ever are exposed as single-stranded regions, this choice reduces potential secondary structure [1]. Sequences for complementary specificity domains were constructed accordingly. Next, subsequences known to be problematic (4 or more G's in a row on complementary domains due to G-quadruplexing, more than 4 A's in a row causing synthesis difficulties, etc.) were altered by hand. The remaining sequences were then concatenated as appropriate to form the DNA strands. These were folded alone and pairwise using the mFold web-server to determine possible spurious bindings [2]. Some bases at problematic subsequences were then changed by hand to G in the primary domains (and propagated elsewhere as appropriate for domain identity), to minimize self-folding and pairwise-folding energies. Finally, the strands were checked again on mFold to ensure minimal spurious interactions [2].

S2. Materials and methods

Substrate purification. Substrate and reporter complexes were manually purified to ensure proper stochiometry and to improve purity. Sources of substrate impurity include synthesis errors and truncations, partially-formed complexes due to imperfect stochiometry, and dimerization. Strands for each sample were prepared with nominally correct stochiometry at 20 μM and annealed. For all substrate complexes except the autocatalyst substrate, the fuel strand was then added, which triggers many poorly-formed substrates to decay into products that can be removed by gel purification. (For the autocatalyst, addition of the fuel strand would have initiated the exponential chain reaction, so the autocatalyst substrate was purified without addition of the fuel strand.) The samples were then run on 12% non-denaturing polyacrylamide gel electrophoresis (PAGE) gel at 180V for 6 hours. The proper bands were cut out and eluted in TE/Mg^{2+} buffer for 2 days. Typical prep sizes ranged from 5 nmol to 10 nmol, and typical elution volume was 2 ml. Typical yields ranged from 40% to 60%. Purified complexes were quantitated by measurement of absorbance at 260 nm, using extinction coefficients for single- and double-stranded DNA predicted by nearest-neighbor models [3].

All annealing processes were performed with an Eppendorf Mastercycler Gradient thermocycler. The samples were brought down from 95 °C to 20 °C at a constant rate over the course of 90 minutes.

DNA oligonucleotides. DNA oligonucleotides used in this study were purchased from Integrated DNA Technologies(IDT), with HPLC purification. Where applicable, fluorophores were attached by IDT as well.

Buffer conditions. The buffer for all experiments was TE (10 mM Tris · HCl pH balanced to 8.0, 1mM EDTA), purchased in 100x stock from Sigma-Aldrich (catalog number T9285), with 12.5 mM $MgCl_2$ added.

Gel electrophoresis. Non-denaturing PAGE was run on 12% acrylamide (19:1 acrylamide:bis), diluted from 40% acrylamide stock purchased from Ambion (catalog number AM9022). ND loading dye containing XCFF in 50% glycerol was added in 0.2x stochiometry to all samples. Gels were run at 25 °C using a Novex chamber with external temperature bath. Gels were stained with Sybr-Gold stain, purchased from Invitrogen (catalog number S-11494), and scanned with a Bio-Rad Molecular Imager. Formation gels shown in Fig. 1C and Fig. 2 were run at 180V for 1 hour.

Total RNA and cell lysate. In the experiment described in Fig. 4B, inset 2, mouse liver total RNA and active rabbit reticulocyte lysate were used. They were both purchased from Ambion (catalog numbers AM7810 and AM1200), as part of their in vitro translation kit. The lysate included exogeneouslly introduced RNAse inhibitor enzymes; we do not expect this to significantly affect the results of the experiment described in Fig. 4B inset 2.

Spectrofluorimetry studies. Spectrofluorimetry studies were done with a commercial SPEX Fluorolog-3 from Horiba. Cuvettes used were 119-004F synthetic quartz cells purchased from Hellma, with total volume 1.6 ml. For studies observing behavior of the TET fluorophore, excitation was at 524 nm, while emissions was at 541 nm. For studies observing behavior of the ROX fluorophore, excitation was at 588 nm, while emissions was at 602 nm. For studies observing behavior of the TAMRA fluorophore, excitation was at 557 nm, while emissions was at 580 nm. Slit size used are 2 nm for both excitation and emission monochrometers for net reaction studies, and 3 nm for individual rate measurements. All experiments were done with integration time of 3 seconds for every 30 second time-point.

Prior to each experiment, all cuvettes were cleaned thoroughly: each cuvette was washed 15 times in distilled water, once in 70% ethanol, another 5 times in distilled water, and finally once more in 70% ethanol.

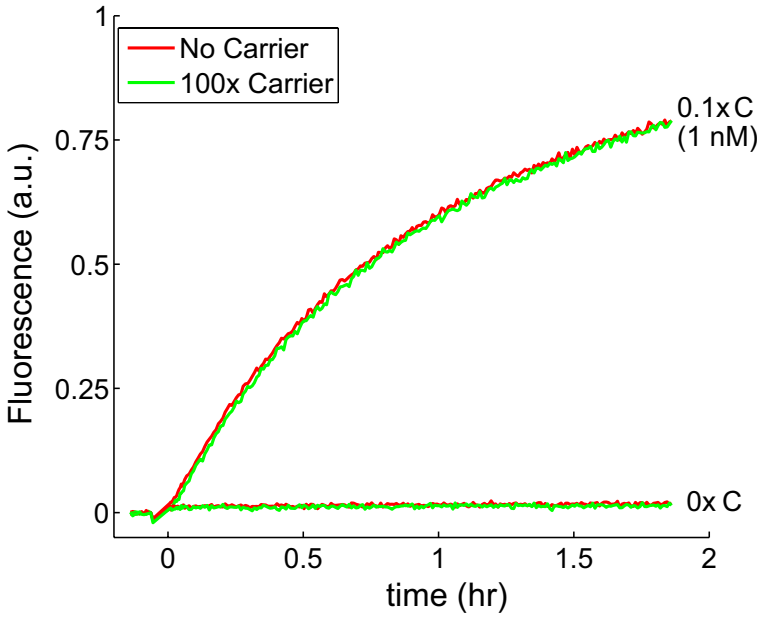

FIG. S1: Non-interaction of poly-T carrier strand. Substrate concentration $[S]$ = 10 nM = 1x (15 pmol at 1.5 ml volume); fuel concentration $[F]$ = 13 nM; 25 °C. Presence of 100x = 1 μM (1.5 nmol for this reaction) of carrier had little effect on kinetics of either catalyzed or uncatalyzed reaction rate.

Fluorescence normalization. All fluorescence experiments show fluorescence values normalized to approximately 1 a.u. = 10 nM. Simulation traces (dotted lines) are offset vertically to correspond to quenched fluorophore baselines. Data traces within a single figure are normalized using the same scaling factor, which was determined by best-fit to simulation traces. Data traces across different figures possess different scaling factors due to differences in fluorescence reporter, lamp luminosity, and substrate concentrations. Time $t = 0$ signals the beginning of the reaction, triggered by the addition of the last necessary reagent (usually the substrate).

Inactivity of carrier strands. In the course of testing the catalyst system and its derivatives, some reactions required very small quantities of certain DNA species. For example, in Fig. 3B (inset), 1 pM of $C0$ in 1.5 ml of solution = 1.5 fmol of DNA. We have experimentally observed that DNA sticks non-specifically to pipette tips, so that direct serial dilutions lead to stocks much more dilute than expected. Unfortunately, this loss is not very consistent, so we could not compensate for tip loss with additional reagent. Instead, we worked around this issue by introducing into all dilute stocks (1 μM and below) a non-reactive 20 nt poly-T "carrier" strand, at a concentration of 1 μM. Since pipette tip loss is non-specific, the majority of DNA loss would be of the carrier strand, so that serially diluted stocks are only slightly more dilute than expected. It is of interest to verify that the carrier strand does not affect kinetics. Thus, we compared performance of the catalyst at concentration ranges where pipette loss is not substantial (see Fig. S1). Presence of the carrier strand appears to have very little, if any, effect on the kinetics of the catalyst, at 100x excess.

S3. Directly-labelled cross-catalyst

This section refers to our earlier attempts at constructing a cross-catalytic network without using the indirect reporting scheme presented in the main paper. Instead, we directly tagged the fuel strand $F3$ with the HEX (Hexachlorofluorescein) fluorophore. As the catalyzed reaction occurs, the fuel strand $F3$ is co-localized with linker strand $LB3$ in the waste product, and the HEX fluorophore is quenched due to its close contact with a guanine (G) base [4]. The sequences of the involved domains are given in Table S1.

Note that the kinetic behavior of cross-catalytic circuit differs substantially from that presented in section S11. First, the reaction is substantially slower, despite being at higher concentrations. Second, the reaction does not quickly go to completion, as the autocatalyst and cross-catalyst circuits presented earlier. We interpret this to be evidence for interaction between the HEX fluorophore and DNA.

S4. Reporter complex characterizations

In the course of this work, we observe kinetics using independent reporter complexes OR and SR; this approach was chosen (rather than direct labelling of strands in the catalyst system) to decouple the thermodynamic effects of fluorophore-quencher binding from the catalytic pathway. Both OR and SR initially contain a 20 bp duplex and a 7 nt toehold domain that uniquely binds their respective targets (OB and SB). Each possesses a different fluorophore

Dom.	Sequence	Length
21	5'- TATTCC -3'	6
22	5'- GCTA -3'	4
23	5'- GTCA -3'	4
24	5'- TACCAA -3'	6
25	5'- CATCG -3'	5
26	5'- ACTACAC -3'	7
27	5'- CTCAG -3'	5
28	5'- CTCAATC -3'	7
29	5'- TACTCTACAC -3'	10
30	5'- CAAATCCTCA -3'	10

Table S1: Domain sequences of HEX-labelled systems

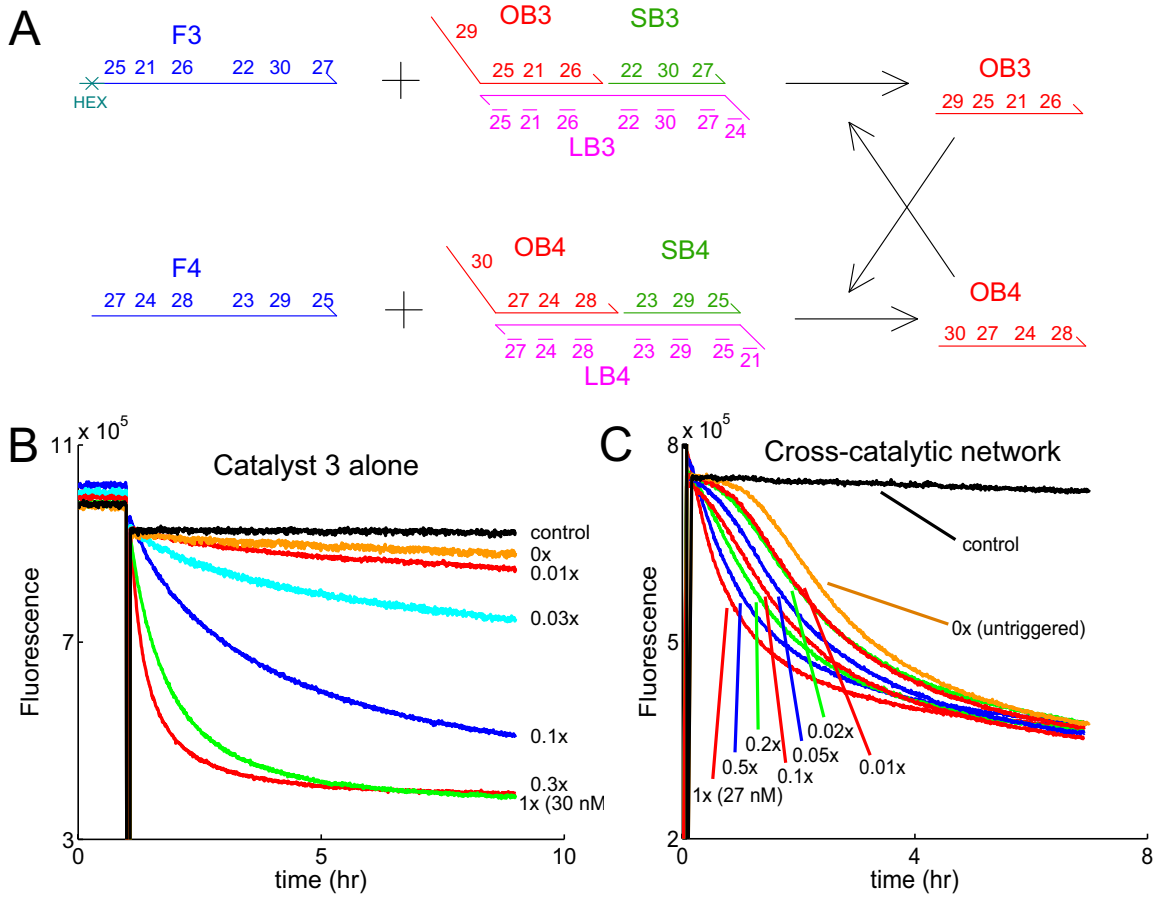

FIG. S2: Directly-labelled cross-catalyst circuit **(A)** Cross-catalyst schematic. HEX represents the hexachlorofluorescein fluorophore, and is quenched by the 3' most base of the the $LB3$ is a guanine (G). **(B)** Test of the F3 + S3 reaction in isolation. $[F3] = [S3] = 30$ nM, $[F4] = [S4] = 0$. Various amounts of catalyst $OB4$ were added at t $\approx$ 1 hour. The catalyzed reaction is substantially slower than that shown in Fig. 1E, despite being at higher concentration. Additionally, the control reaction (which lacked substrate $S3$) showed some decrease of signal over the observed time; this is suspected to be fluorophore bleaching. These were the earliest experiements we ran, and technical proficiency for these experiments were not as high as for other results. Normalization was not performed for these reactions because it is not clear where endpoints were. **(C)** Cross-catalyst series. $[F3] = [F4] = [S3] = [S4] = 27$ nM. Only catalyst $OB3$ was added at t $\approx$ 0.

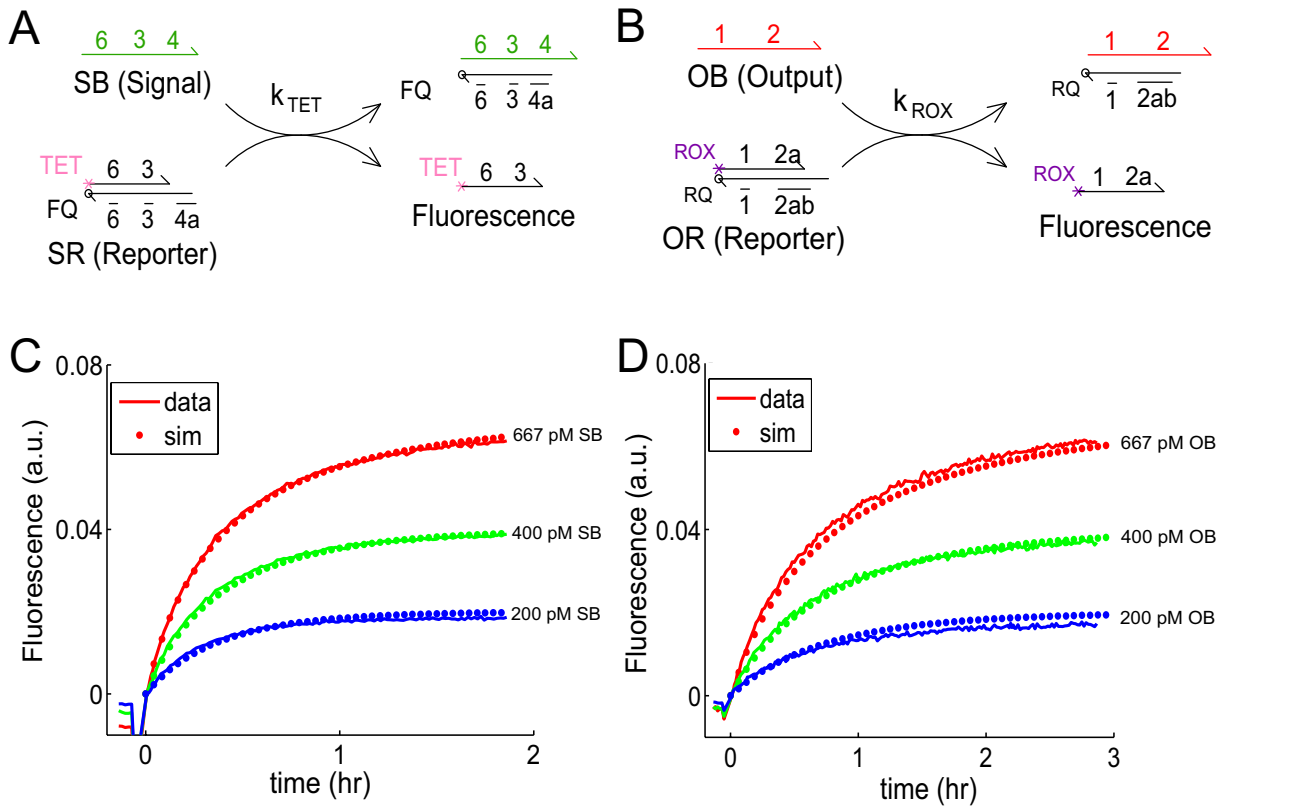

FIG. S3: Reference experiments. **(A)** Schematic of signal (SB) reporter using TET and Iowa Black Fluorescence Quencher (FQ). **(B)** Schematic of output (OB) reporter using ROX and Iowa Black Red Quencher (RQ). **(C)** Displacement rate of strand SF by SB at 25 °C. Reporter complex SR was present in solution at 1 nM at t=0, and various amounts of SB were added at t ≈ 0. Dotted lines show simulation traces of a second-order displacement reaction with rate constant $k_{TET} = 8 \cdot 10^5 M^{-1}s^{-1}$. **(D)** Displacement rate of strand OF by OB at 25 °C. Reporter complex OR was present in solution at 1 nM at t=0, and various amounts of OB were added at t ≈ 0. Dotted lines show simulation traces of a second-order displacement reaction with rate constant $k_{ROX} = 4 \cdot 10^5 M^{-1}s^{-1}$.

and quencher pair (TET and Iowa Black Fluorescence Quencher (FQ) for SR; ROX and Iowa Black Red Quencher (RQ) for OR). The reactions are assumed to be non-reversible:

$$SB + SR \overset{k_{TET}}{\rightarrow} Fluorescence \tag{1}$$

$$OB + OR \overset{k_{ROX}}{\rightarrow} Fluorescence \tag{2}$$

Displacement rate constants of the two reporter complexes OR and SR were measured via fluorescence at initial reactant concentrations of 1 nM ($\frac{1}{30}$ the concentration used in catalyst experiments) to be $k_{TET} = 8 \cdot 10^5 M^{-1}s^{-1}$ and $k_{ROX} = 4 \cdot 10^5 M^{-1}s^{-1}$ (see Fig. S3). The observed difference in displacement rate constants may be due to either the thermodynamics of the fluorophore/quencher pairs, differences in binding strength of the toehold domains, or secondary structure differences in SB and OB.

S5. Catalyst modelling and characterization

As described in the main paper, we are able to predict the net behavior of the catalyst system using a reduced model of the catalytic pathway. The reactions of three-step process are redisplayed below.

$$S + F \overset{k_0}{\rightarrow} OB + SB + W \tag{3}$$

$$S + C \underset{k_{-1}}{\overset{k_1}{\rightleftharpoons}} I3 + SB \tag{4}$$

$$I3 + F \overset{k_2}{\rightarrow} I5 + OB \tag{5}$$

$$I5 \underset{k_{-3}}{\overset{k_3}{\rightleftharpoons}} C + W \tag{6}$$

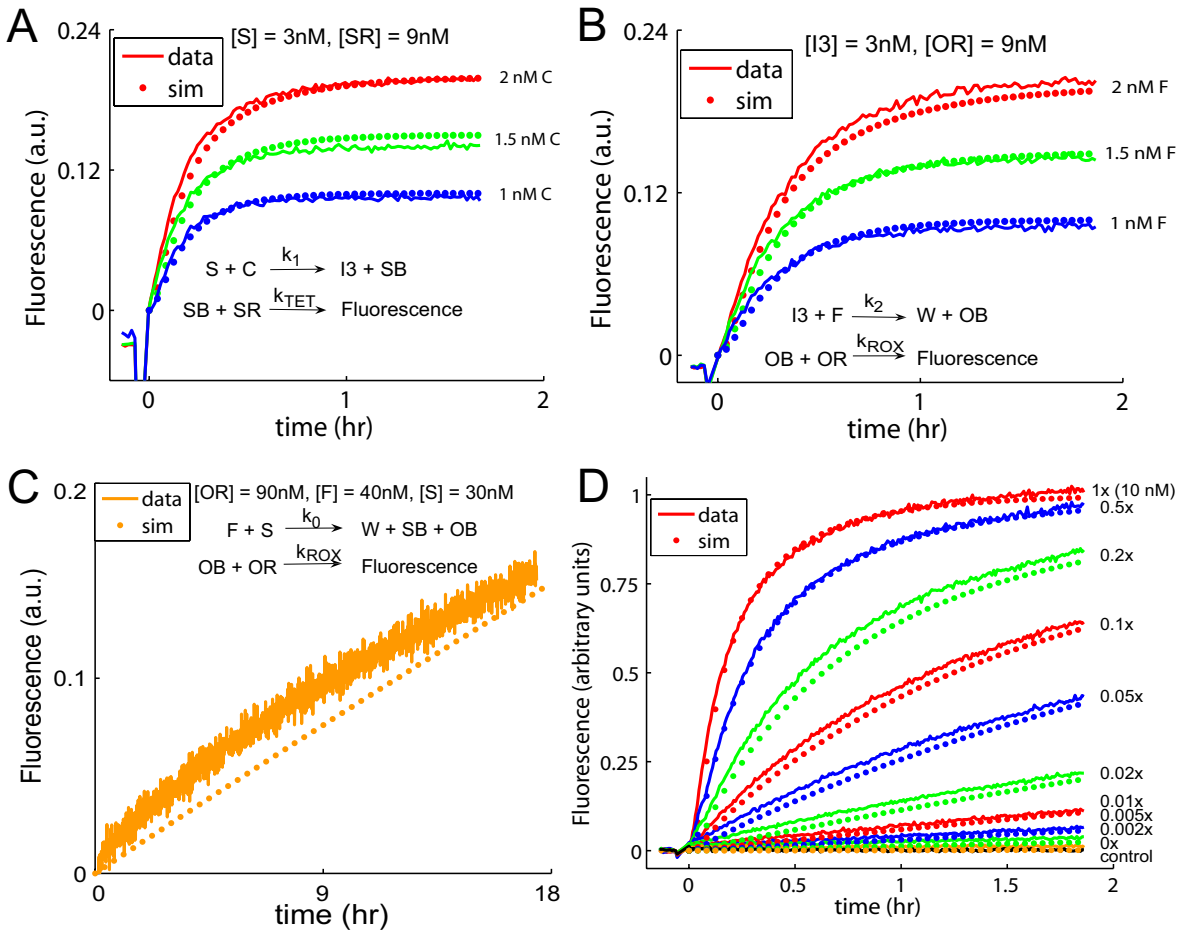

FIG. S4: Intermediate rate measurements. **(A)** Measurement of catalyst binding rate k_1. All traces contain 3 nM S initially, and different amounts of C were added at $t \approx 0$. Reporter SR was present at 9 nM concentration. Dotted lines show simulation traces modelling reactions (1) and (4), assuming rate constant $k_1 = 6.5 \cdot 10^5 M^{-1}s^{-1}$ **(B)** Measurement of fuel binding rate k_2. All traces contain 3 nM pre-prepared $I3$ initially, and different amounts of F were added at $t \approx 0$. Reporter OR was present at 9 nM concentration. Dotted lines show simulation traces modelling reactions (2) and (5), assuming rate constant $k_2 = 4.2 \cdot 10^5 M^{-1}s^{-1}$ **(C)** Measurement of uncatalyzed reaction rate k_0. $[S] = 30$ nM, $[F] = 40$ nM, and no catalyst was present. Reporter OR was present at 90 nM concentration. Dotted lines show simulation traces modelling reactions (2) and (3), assuming rate constant $k_0 = 2.3 \cdot 10^1 M^{-1}s^{-1}$ **(D)** Data vs. simulation using measured rates, repeated from main text. Rate constant $k_3 = 4 \cdot 10^{-3}s^{-1}$ was fitted.

Using symmetry and our understanding of DNA binding thermodynamics, we are able to approximate two of the parameters: First, the spurious re-assocation rate of C and W is initiated by the same external 6 nt $\bar{5}$ domain as the correct association of C to substrate S, and consequently the rate constants should be similar. Thus, we assume for our simulations that $k_{-3} = k_1$. Second, the back-reaction of $I3$ and SB to re-form S and C is initiated by the same internal domain $\bar{5}$ (of length 4 nt) as the correct association of F to intermediate $I3$, so we assume that $k_{-1} = k_2$.

Using k_{TET} and k_{ROX} rate constants from the previous section, reaction rate constants k_1, k_2, and k_0 are directly measured to be $6.5 \cdot 10^5$, $4.2 \cdot 10^5$, and $2.3 \cdot 10^1 M^{-1}s^{-1}$, respectively (see Fig. S4). Note that for these experiments, we can effectively ignore the k_{-1} rate of reverse reaction $SB + I3$, because SB was consumed by reporter complex SR (simulations showed no visible difference when k_{-1} was modeled). The last rate constant k_3 is difficult to measure because it is first-order, and we could not slow it down to the time-scale where our spectrofluorimeter readings are meaningful. Thus, it was fitted using the results of the net kinetics of the catalytic system to be $4 \cdot 10^{-3}s^{-1}$. Fig. 1E is redisplayed here as Fig. S4D.

S6. Estimates of Entropy and Free Energy

We consider the net reaction

$$S + F \rightleftharpoons OB + SB + W$$

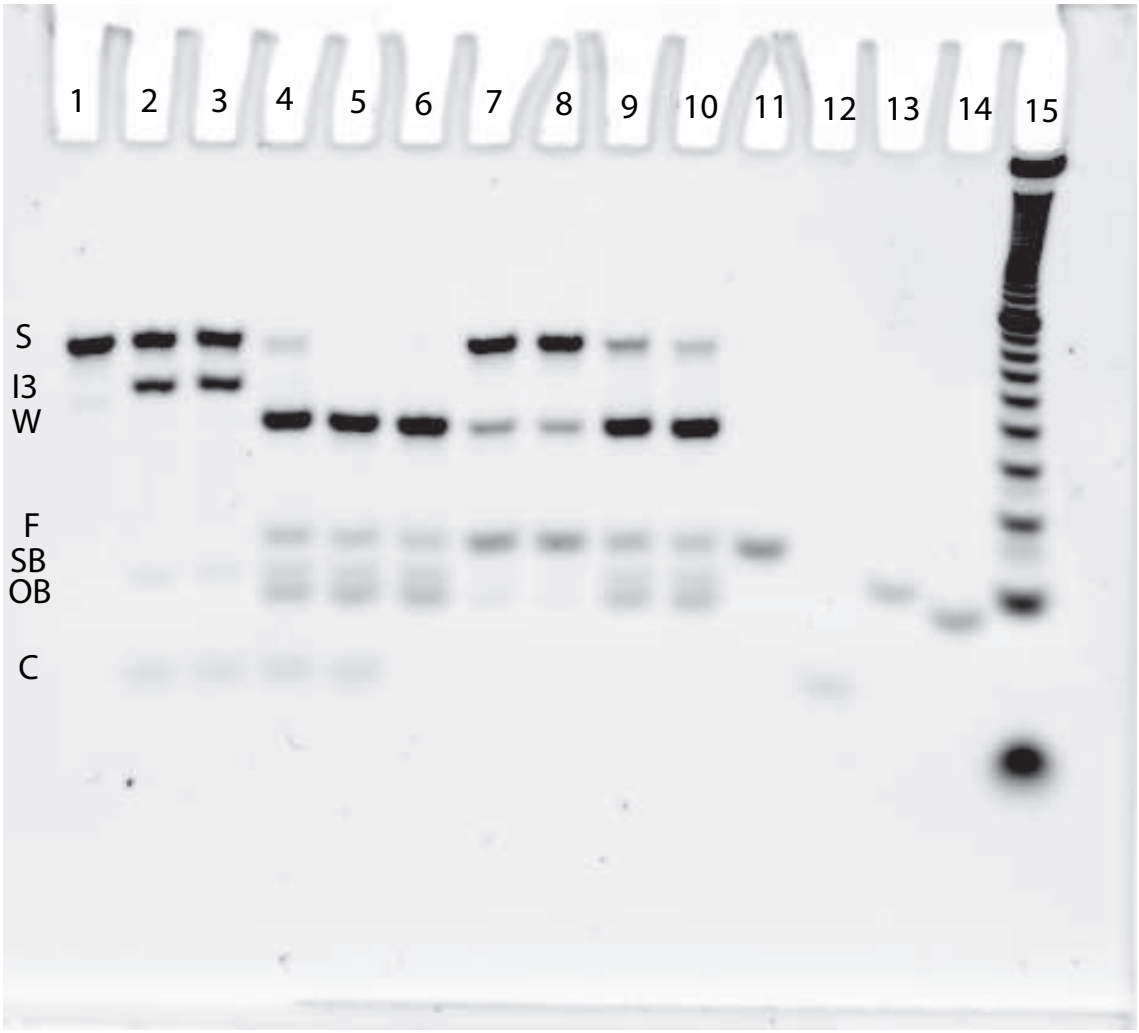

FIG. S5: Full formation gel including control lanes. 25 °C, 1x = 200 nM, 12% non-denaturing (native) PAGE. This is the full version of the cropped gel in Fig. 1C. Note that Sybrgold stains single-stranded DNA much less efficiently than double-stranded DNA, so that relative brightness between different bands should not be compared.
L1: S [1x].
L2: S [1x] + C [1x], 30 min.
L3: (S [1x] + C [1x]).
L4: (S [1x] + C [1x]) + F [1x], 30 min.
L5: (S [1x] + C [1x] + F [1x]).
L6: (S [1x] + F [1x]).
L7: S [1x] + F [1x], 30 min.
L8: S [1x] + F [1x], 180 min.
L9: S [1x] + F [1x] + C [0.1x], 30 min.
L10: S [1x] + F [1x] + C [0.1x], 180 min.
L11: F [1x].
L12: C [1x].
L13: SB [1x].
L14: OB [1x].
L15: 10 nt duplex ladder.
Parentheses denote that the included species were annealed together.

The free energy change for this reaction, in dilute solutions, is

$$\Delta G = \Delta G^\circ_{OB} + \Delta G^\circ_{SB} + \Delta G^\circ_W - \Delta G^\circ_S - \Delta G^\circ_F + RT \ln Q \stackrel{\text{def}}{=} \Delta G^\circ_{net} + RT \ln Q$$

where $Q = ([OB]/c^\circ \cdot [SB]/c^\circ \cdot [W]/c^\circ)/([S]/c^\circ \cdot [F]/c^\circ)$ is the reaction quotient relative to standard conditions and ΔG°_X is the standard free energy of species X at standard conditions, which here specify our TE buffer with 12.5 mM magnesium, 25 °C, and $c^\circ = 1$ M.

The free energy change (the driving force for the reaction) decreases as concentrations change during the course of the reaction; once equilibrium is achieved, $Q = \exp\{-\Delta G^\circ_{net}/RT\}$ and $\Delta G = 0$. If the standard free energy change $\Delta G^\circ_{net} \approx 0$, as we expect for the reaction with the full-length fuel strand if the standard free energy is dominated by base pairing, then the driving force at any moment is just $RT \ln Q$. As a somewhat arbitrary reference point, we consider the time at which half the substrate has been depleted. For the reaction in Fig. 2, this occurs when $[S] = [F] = [SB] = [OB] = [W] = c = 100$ nM, $Q = 10^{-7}$, and $RT \ln Q = RT \ln c = -9.6$ kcal/mol. For the reaction in Fig. 1E, $c = 5$ nM and $RT \ln c = -11.4$ kcal/mol.

The free energy difference between the substrate S and the maximally truncated waste product W was approximated using the mFold server [2] using DNA parameters for 25 °C, with salt conditions being 10 mM Na^+ and 12.5 mM Mg^{2+}. Taking into consideration the 8 base pair stacks, external loops and dangles (due to the 1 domain in S, and the 3' overhang on the LB strand on the truncated waste product W), and an initiation entropy of 6.4 cal/mol/K per association, the predicted standard free energy change ΔG°_{net} for the (unfavorable) forward reaction is +11.7 kcal/mol.

According to these estimates, truncating the fuel strand F by 8 bases should disfavor the forward reaction enough that the equilibrium distribution possesses substrate S in excess of waste W. However, the experiments described in Fig. 2 show waste in excess of substrate after 3 hours. This suggests that the estimate for ΔG°_{net} is too large; a value closer to +9 would be more compatible with the experiments.

S7. Catalyst robustness to temperature and salt conditions

As mentioned in the main text, we expect the entropy-driven catalytic reaction design to be somewhat more robust to changes in environmental conditions, such as temperature and salt concentrations. Salt conditions affect the free energy of hybridization [5], but since there is no net gain or loss of base-pairs in a net reaction cycle, the equilibrium should not be significantly affected. The strength of the binding of the toehold domains still depend on the free energy of the base pairs formed, so salt concentration will affect the kinetics of the catalyzed pathway. However, the catalyst should qualitatively function across the range of salt concentrations, as long as the toehold domains still are able to co-localize the relevant strands. In Fig. S6A, we see that catalytic function is preserved across a broad range of salt buffers, but degrades for sufficiently low salt concentrations.

Temperature affects the equilibrium of a reaction only through the enthalpic change (ΔH°). When the magnitude of the enthalpic change is small ($\Delta H^\circ \approx 0$) as it is for the entropy-driven system, the effects of temperature have little effect on the reaction equilibrium – although, again, they affect the kinetics of toehold-mediated processes. In Fig. S6B, the catalyst is shown to function across a 25 degree range of temperatures, from 12 °C to 37 °C.

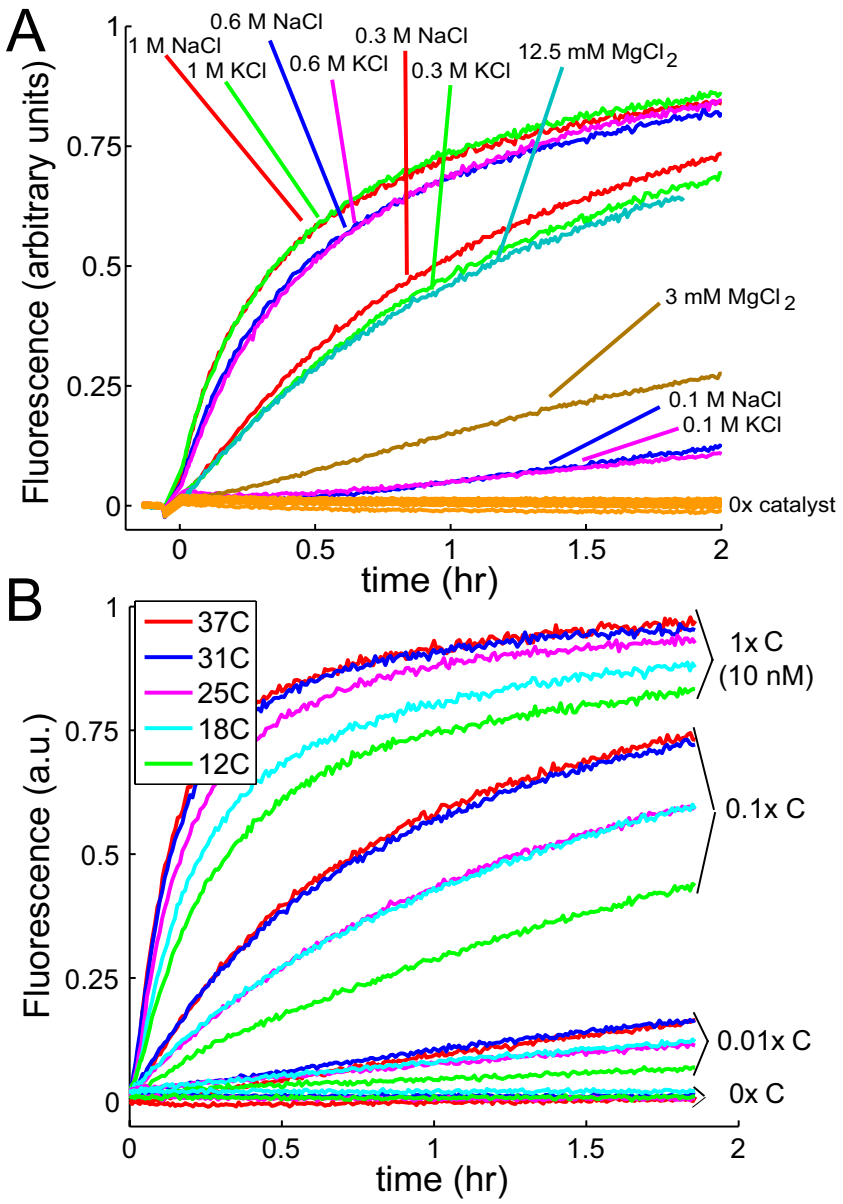

FIG. S6: Robustness of entropy-driven catalytic reaction shown in Fig. 1. **(A)** Salt condition robustness. The same system as presented in Fig. 1 was tested here in TE supplemented with various different salt concentrations. $[S] = 10$ nM and $[F] = 13$nM. The orange traces at the bottom (controls run for every salt condition tested) show $[C] = 0$, while all other traces have $[C] = 1$ nM $= 0.1$x. Reactions were run at 25 °C. Catalysis functions with fast kinetics over a broad range of salt conditions. All traces shown normalized to the same scaling factor. **(B)** Temperature robustness. Catalysis functions qualitatively similar across temperatures from 12 °C to 37 °C. Reactions were run in TE with 12.5 mM $MgCl_2$. Note that the 18 °C and 25 °C traces show very similar kinetics for 0.1x C and 0.01x C, as do the 31 °C and 37 °C traces. To account for temperature-dependent fluorescence, traces were normalized individually with separate experiments (data not shown) that measured the fluorescence of the ROX fluorophore at different temperatures. We do not have an explanation for the near-superposition of some traces run under different conditions.

S8. Details of quadratic feedforward circuit and autocatalyst

Domain sequences. The domains involved in the quadratic feedforward circuit (Fig. 3) and the autocatalytic reaction (Fig. 4) are shown below in Table S2. As mentioned in the main text, there is a significant amount of domain redundancy, because the initial catalyst, quadratic circuit, and autocatalyst circuit were designed simultaneously with the goal of minimizing the number of changes between designs. Again, we stress that in designing a catalytic reaction system in isolation, the domains may be completely independent (see section S10).

Domains $2a$, $4b$, and $9b$ are identical to each other, and are also referred to as x in the cross-catalytic schematic (see Fig. S10). Domains $2b$, 5, and 10 are identical to each other, and are also referred to as y in the cross-catalytic schematic.

Quadratic feedforward circuit fits. For the feedforward circuit, the model presented in the main paper is expanded to include one separate set of equations for each layer:

$$S0 + F0 \xrightarrow{k_{00}} OB0 + SB0 + W0 \tag{7}$$

$$S0 + C0 \underset{k_{-10}}{\overset{k_{10}}{\rightleftharpoons}} I30 + SB0 \tag{8}$$

$$I30 + F0 \xrightarrow{k_{20}} I50 + OB0 \tag{9}$$

$$I50 \underset{k_{-30}}{\overset{k_{30}}{\rightleftharpoons}} C0 + W0 \tag{10}$$

$$S1 + F1 \xrightarrow{k_{01}} OB1 + SB1 + W1 \tag{11}$$

$$S1 + OB0 \underset{k_{-11}}{\overset{k_{11}}{\rightleftharpoons}} I31 + SB1 \tag{12}$$

$$I31 + F1 \xrightarrow{k_{21}} I51 + OB1 \tag{13}$$

$$I51 \underset{k_{-31}}{\overset{k_{31}}{\rightleftharpoons}} C1 + W1 \tag{14}$$

$$\tag{15}$$

As mentioned in the main text, the downstream layer catalyst system is identical to that presented in Fig. 1C, and thus we use the same rate parameters for it as used in Fig. 1E: $k_{01} = 2.3 \cdot 10^1 M^{-1}s^{-1}$, $k_{11} = k_{-31} = 6.5 \cdot 10^5 M^{-1}s^{-1}$, $k_{-11} = k_{21} = 4.2 \cdot 10^5 M^{-1}s^{-1}$, $k_{31} = 4 \cdot 10^{-3} s^{-1}$. The remaining parameters for the upstream catalyst system are fitted to the quadratic series data, with the same constraints $k_{10} = k_{-30}$ and $k_{-10} = k_{20}$. The dotted traces displayed in Fig. S7C show $k_{10} = k_{-30} = 5.0 \cdot 10^5 M^{-1}s^{-1}$, $k_{11} = k_{21} = 1.9 \cdot 10^5 M^{-1}s^{-1}$, and $k_{30} = 8 \cdot 10^{-3} s^{-1}$. Note that the rates are quantitatively similar (though somewhat slower) to the rates of the analogous reactions in the upstream system, which supports our understanding of the behavior of the circuit.

As seen in the gel in Fig. 1C, some impurity fraction of the substrate S reacts very quickly to fuel F. Evidence for this is also seen in Fig. 1E, where the fluorescence value of the yellow "0x" trace is slightly higher after the addition of fuel F at $t \approx 0$. For the quadratic feedforward circuit, a small constant amount of $OB0$ released from the upstream system would be converted into a small constant production rate of $OB1$. We fitted this initial concentration $[OB0]$ to be 45 pM, for a total of 4 additional fitted parameters.

Dom.	Sequence	Length
1	5'- CTTTCCTACA -3'	10
2a (=x)	5'- CCTACG -3'	6
2b (=y)	5'- TCTCCA -3'	6
2c	5'- ACTAACTTACGG -3'	12
3	5'- CCCT -3'	4
4a	5'- CATTCAATAC -3'	10
4b (=x)	5'- CCTACG -3'	6
5 (=y)	5'- TCTCCA -3'	6
6	5'- CCACATACATCATATT -3'	16
7	5'- TACTTATTAGCC -3'	12
8	5'- GACA -3'	4
9a	5'- CTACTTTCAC -3'	10
9b (=x)	5'- CCTACG -3'	6
10 (=y)	5'- TCTCCA -3'	6

Table S2: Domain sequences

Autocatalytic feedback circuit fits. For the autocatalytic system, we use reporter complex SR to measure the

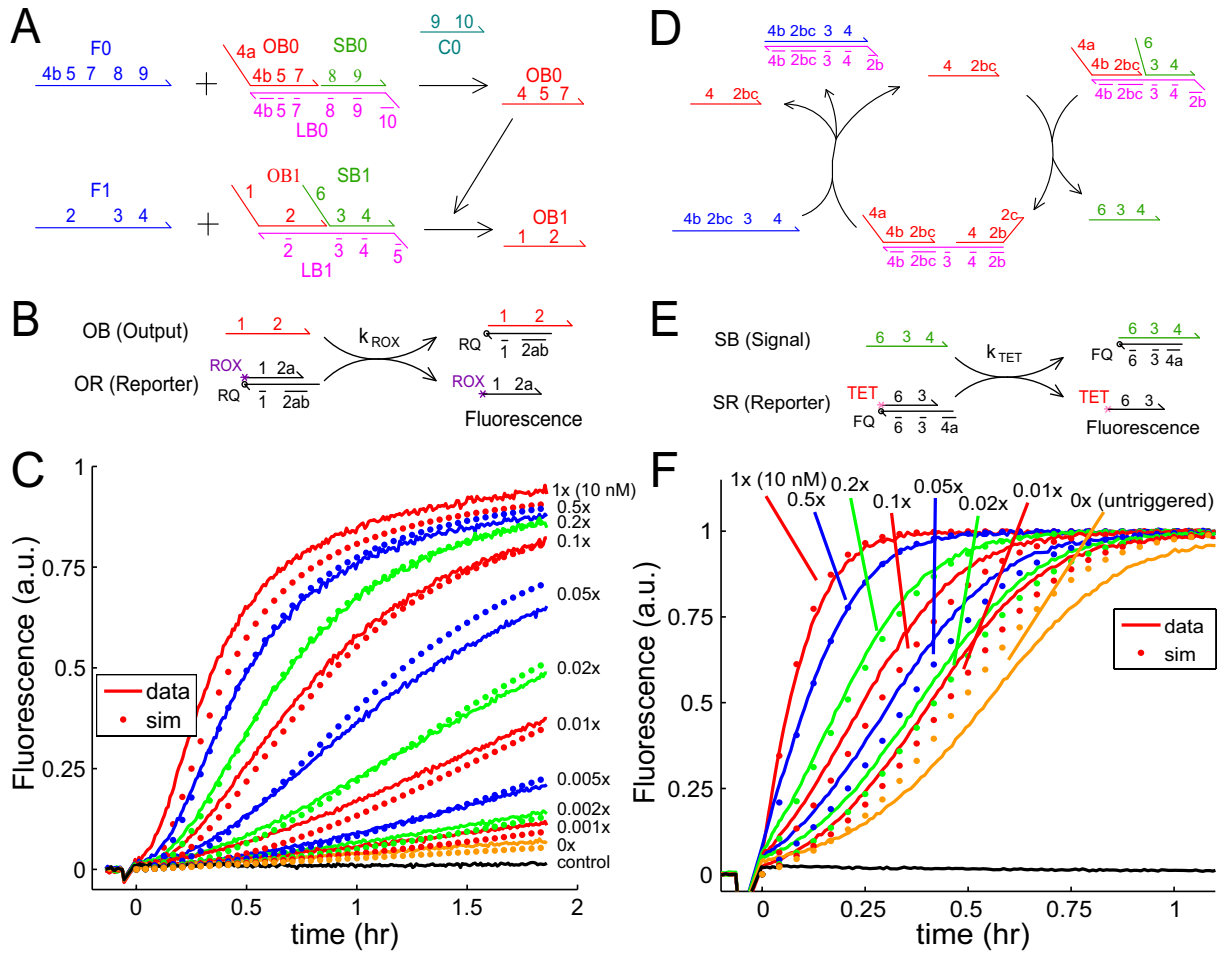

FIG. S7: Fitting the feedforward circuit and the autocatalytic reaction. **(A)** Schematic of the feedforward circuit. **(B)** Schematic of the reporter OR used for the feedforward circuit (same as displayed in Fig. 1D). **(C)** Fits to the quadratic circuit using fitted parameters described in text. **(D)** Schematic of the autocatalytic reaction. **(E)** Schematic of the reporter SR used for the autocatalytic reaction and the cross-catalytic circuit. **(F)** Fits to the autocatalytic reaction using the fitted parameter for the initial $[OB]$, as described in the text.

progress of the reaction, because we do not wish to damp the exponentiation by reacting OB with OR. A schematic for the reaction is shown in Fig. S7E. The reaction set we use to model the behavior of the autocatalyst is shown below:

$$SB + SR \xrightarrow{k_{TET}} Fluorescence \tag{16}$$

$$S + F \xrightarrow{k_0} OB + SB + W \tag{17}$$

$$S + OB \underset{k_{-1}}{\overset{k_1}{\rightleftharpoons}} I3 + SB \tag{18}$$

$$I3 + F \xrightarrow{k_2} I5 + OB \tag{19}$$

$$I5 \underset{k_{-3}}{\overset{k_3}{\rightleftharpoons}} OB + W \tag{20}$$

Parameters k_{TET}, k_0, k_1, k_{-1}, k_2, and k_{-3} again are the same as measured previously. Parameter $k_3 = 4 \cdot 10^{-3} s^{-1}$ is the same as fitted to the catalyst data in Fig. 1E. The only new parameter fitted is the impurity concentration, the initial concentration of $[OB] = 460$ pM. Purification of the autocatalyst substrate was significantly more difficult technically than that of the catalyst substrate, as evidenced by different inferred initial $[OB]$ for different purified samples.

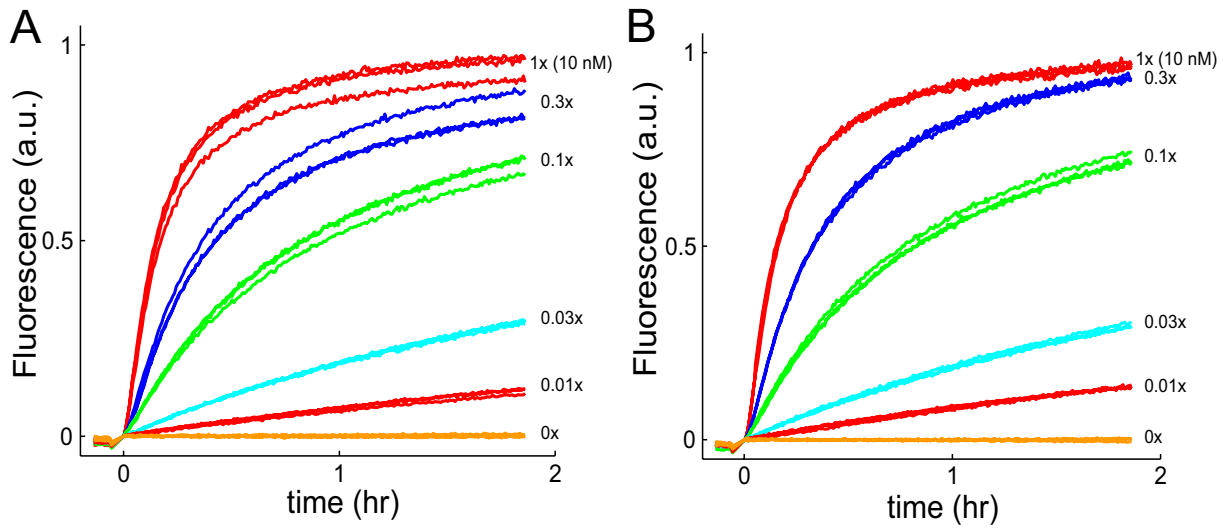

FIG. S8: Repeatability of fluorescence traces. **(A)** Repeatability of experiments before optimization of protocol. The traces are of the catalyst system shown in Fig. 1. **(B)** Repeatability of experiments after optimization.

S9. Repeatability of fluorescence experiments

Several factors reduced the repeatability of fluorescence experiments: First, the spectrofluorimeter luminosity output differs from lamp bulb to lamp bulb and luminosity tends to decrease as any particular lamp bulb ages. Second, different preparations of purified substrate complexes S, though nominally calibrated to the same concentration, in practice differed in purity. Third, fluorophores tend to bleach, and thus older stocks tend to give lower fluoroscence readings for the same concentration. Finally, our Eppendorf pippetors are high precision but low accuracy; thus using two different pipetors to measure the same volume would often yield different pippetted quantities.

The effects of the above on repeatability is shown in Fig. S8: Fig. S8A shows repeatability of experiments before implementing measures to combat any of the above (traces agree to within 15%), while Fig. S8B shows repeatability of experiments after implementing measures (traces agree to within 3%). In summary, the following were done for all fluorescence experiments displayed in the main text:

1. All traces within a figure were performed in a single sitting, one right after another.
2. All traces within a figure used the same stocks of all purified samples, including reporter complexes and substrate complexes.
3. All traces within a figure used the exact same pipettor for each quantity measured (i.e. dedicated pipettor for 6 μl, another dedicated pipettor for 15 μl, etc).

S10. Catalyst system with independent input/output sequences

In the example system presented in Fig. 1 of the main text, domains $2b$ and 5 are identical, so strands C and OB are not independent. However, this is not essential; the design was chosen to minimize the number of changes needed to explain the autocatalyst design. A design in which OB and C possess independent sequences is demonstrated here (see Fig. S9). The sequences of the system are shown in Table S3. This catalyst system functions almost identically as the one presented in Fig. 1A.

Modularity is facilitated by sequence independence of the input (catalyst) and output (product); it is for this reason that we do not label strand SB also an output, even though it is also catalytically released by C. The design of the catalysis reaction enforces some degree of sequence similarity between strands SB and C, and this limits its usefulness in the construction of larger-scale circuits.

S11. Cross-catalytic feedback circuit

The main text refered to experiments on a cross-catalytic feedback circuit. A schematic of the circuit is shown in Fig. S10A. Recall that domains $2a$, $4b$, and $9b$ are identical to each other, and renamed x here. Domains $2b$, 5, and 10 are identical to each other, and renamed y here. Thus, the design is actually very similar to that of the feedforward quadratic circuit, the only difference being that the the $OB1$ output strand has been replaced by $OB1E$, possessing the $9a$ domain at its 5'-most end, rather than the 1 domain.

Strand	Length	Domain Abstraction	Sequence
IndCat-F	44	12 13 14 15	5'- ACCACATCAA TCTCGATCCAGTAC ACCT CTTCACGAACATTTCA -3'
IndCat-LB	50	$\bar{16}$ $\bar{15}$ $\bar{14}$ $\bar{13}$ $\bar{12}$	5'- TGGCTA TGAAATGTTCGTGAAG AGGT GTACTGGATCGAGA TTGATGTGGT -3'
IndCat-SB	20	14 15	5'- ACCT CTTCACGAACATTTCA -3'
IndCat-OB	34	11 12 13	5'- ACCTAATAGC ACCACATCAA TCTCGATCCAGTAC -3'
IndCat-C	22	15 16	5'- CTTCACGAACATTTCA TAGCCA -3'
IndCat-OF2	20	F 11 12	5'- /TAMRA/ ACCTAATAGC ACCACATCAA -3'
IndCat-OQ2	27	$\bar{13}t$ $\bar{12}$ $\bar{11}$ Q	5'- ATCGAGA TTGATGTGGT GCTATTAGGT /IAbRQ/ -3'

Table S3: Independent input/output catalyst system sequences

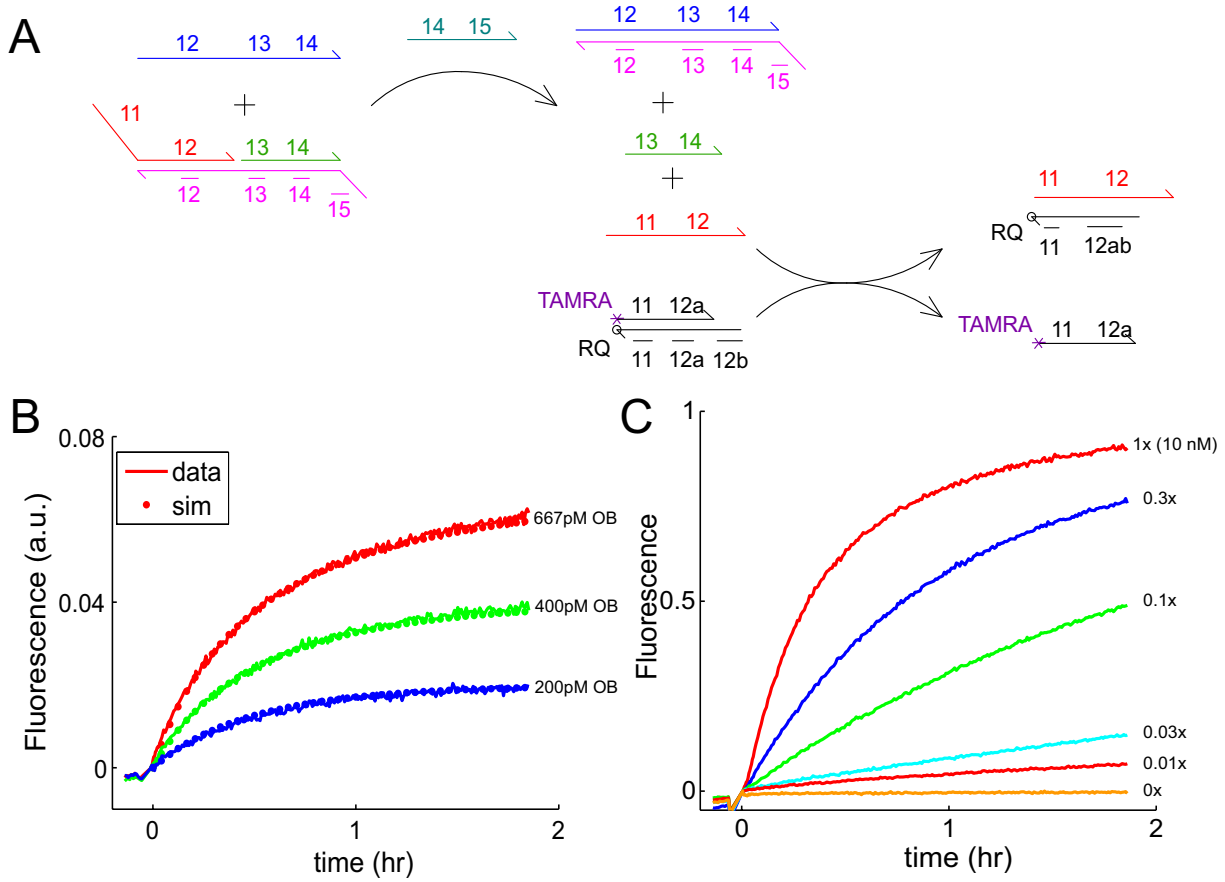

FIG. S9: Catalyst system with independent input/output sequences. **(A)** Schematic of catalyst system, including fluorescence reporter. Strands are labelled by function as shown in Fig. 1A. **(B)** Characterization of reporter. Reporter complex was present in 1 nM concentration; various amounts of output were added. Dotted lines show simulation traces (normalized) assuming second-order displacement rate $k_{TAMRA} = 6 * 10^5 M^{-1} s^{-1}$ **(C)** Catalytic series at $[S] = 10$ nM $= 1$x, $[F] = 13$ nM $= 1.3$x.

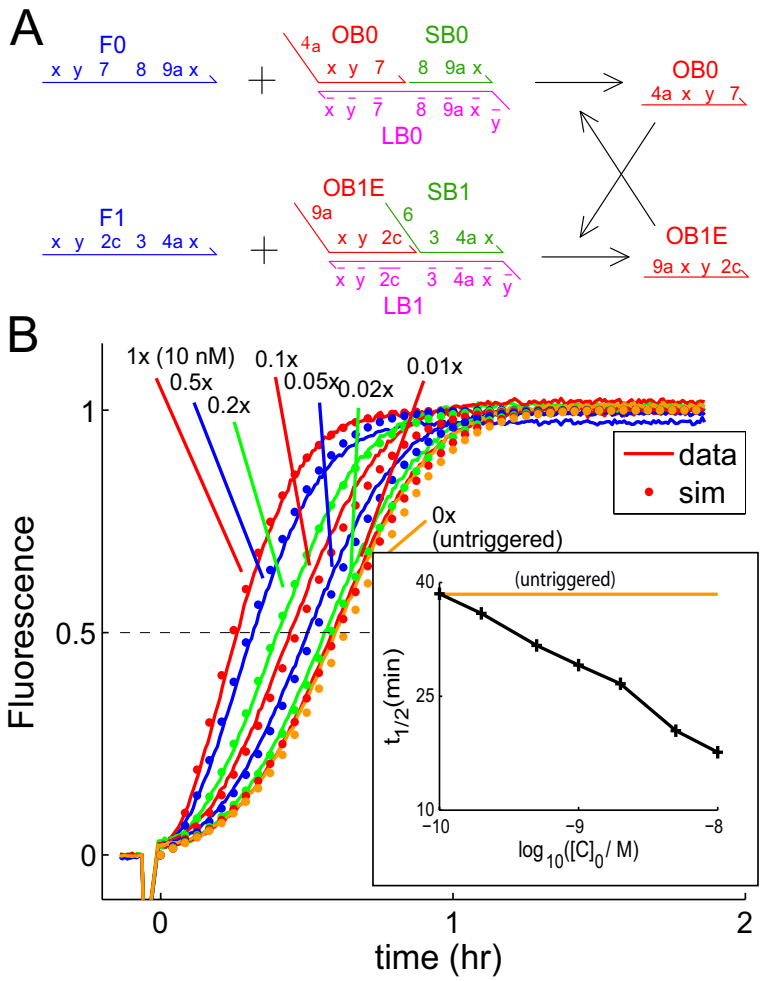

FIG. S10: Cross-catalyst circuit **(A)** Cross-catalyst schematic. **(B)** Cross-catalyst series. Fluorescence studies were performed using the *SR* reporter complex shown in Fig. S3A (same as that used for autocatalyst). Only catalyst *OB1E* was added at t ≈ 0. **(Inset)** Semi-log plot of time to reaction half completion as a function of catalyst added.

Kinetic data from fluorescence studies is shown in Fig. S10B. The cross-catalyst system is more leaky than the autocatalyst system, and 1% trigger is indistinguishable from the untriggered reaction. The reactions used in the modelling of the cross-catalyst system are shown below:

$$S0 + F0 \overset{k_{00}}{\rightarrow} OB0 + SB0 + W0 \tag{21}$$

$$S0 + OB1E \underset{k_{-10}}{\overset{k_{10}}{\rightleftharpoons}} I30 + SB0 \tag{22}$$

$$I30 + F0 \overset{k_{20}}{\rightarrow} I50 + OB0 \tag{23}$$

$$I50 \underset{k_{-30}}{\overset{k_{30}}{\rightleftharpoons}} OB1E + W0 \tag{24}$$

$$S1 + F1 \overset{k_{01}}{\rightarrow} OB1 + SB1 + W1 \tag{25}$$

$$S1 + OB0 \underset{k_{-11}}{\overset{k_{11}}{\rightleftharpoons}} I31 + SB1 \tag{26}$$

$$I31 + F1 \overset{k_{21}}{\rightarrow} I51 + OB1E \tag{27}$$

$$I51 \underset{k_{-31}}{\overset{k_{31}}{\rightleftharpoons}} C1 + W1 \tag{28}$$

$$\tag{29}$$

The only difference between the cross-catalytic circuit and the feedforward circuit is the identity of the 5' domain of the $OB1$ strand; this difference should not affect any rate constants, so the rate constants used in simulations are exactly the same as those used for the quadratic feedforward circuit. The only additional parameter we need to fit is the effective initial concentrations of $OB0$ and $OB1E$. Fig. S10B shows the fits with initial concentrations $[OB0] = [OB1E] = 280$ pM. It is not clear why the impurity of these substrates is higher than that of the quadratic feedforward circuit.

S12. Entropy-driven catalytic analog AND gate

In this section, we demonstrate a reaction mechanism for a catalytic analog AND gate. Fig. S11A shows a reduced schematic of the function of the AND gate: Fuel strands 32-33-34-1 and 2-3-4 (not shown) displace the 5' and 3' regions of the output strand 34-1-2 from the respective linking strands, and these reactions are catalyzed by strands 31-32 and 4-5. When both the 5' and 3' ends of the output strand are released, it reacts with the reporter complex (same as in Fig. 1D of main text) and fluorescence increases.

The multiplicative (AND-like) behavior can be understood quantitatively as follows. The left (5') and right (3') catalytic ends operate independently and follow approximately the same kinetics as the catalyst system of Fig. 1. Let $f_L(t)$ be the fraction of left ends that have reacted with the fuel strand 32-33-34-1, and let $f_R(t)$ be the fraction of right ends that have reacted with the fuel strand 2-3-4. Then the fraction of output strand that has been released on both ends, and thus made active, is $f_{out}(t) = f_L(t) \cdot f_R(t)$. At initial times, when catalytic activity is linear in catalyst strand concentrations x and y, we thus have $f_{out}(t) \approx Mxyt^2$ for some constant M. Consequently, at a fixed time (prior to saturation), the output concentration is proportional to the product of the input concentrations.

As the 3' region of the output and the substrate are very similar to the system given in Fig. 1, the same reaction rates were used here for simulation. For the reaction rates relevant to the 5' catalytic component, the same rate constants were used as for the quadratic feedforward circuit, taken as "typical" values. That is, the reactions rates were not fitted to the data given here, even though the reaction rates most likely differ, since the sequences for the left end of the AND gate are quite different from those of the upstream catalyst of the quadratic circuit. New domain sequences are given in Table S4.

Dom.	Sequence	Length
31	5'- CACACA -3'	6
32	5'- ACTTCAGTCATTAAGC -3'	16
33	5'- AGAC -3'	4
34	5'- CCATACAAGTATCA -3'	14

Table S4: New domain sequences for the catalytic analog AND gate

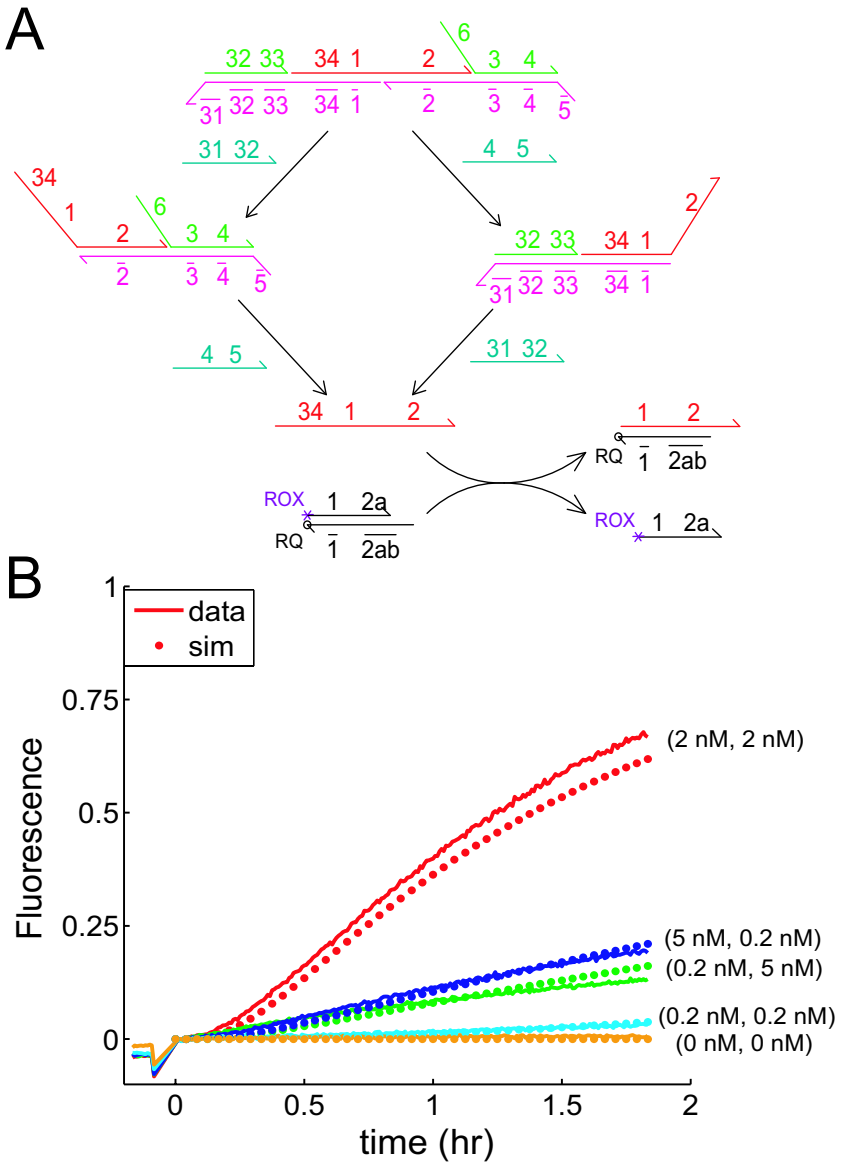

FIG. S11: Catalytic AND gate. **(A)** Schematic of function. The output strand (34-1-2) is sequestered on both the 5' and 3' ends in the substrate. The catalysts 31-32 and 4-5 function independently to release the 5' and 3' ends, respectively, of the output. This action requires fuel strands 32-33-34-1 and 2-3-4 (not pictured). Only when both ends are released is the output strand able to react with the reporter complex. (In the right-hand pathway, single-stranded domain 2 can interact with the reporter complex, but initiation of four-way branch migration through helical domains 1, which could in principle complete triggering of the reporter, is sufficiently slow as to be negligible in practice.) The design is symmetric, despite appearances; domains 34 and 1 always appear together, and their lengths sum to the same as that of domain 2 (24 nt). (They labeled separately only for historical reasons to clarify interactions with the reporter complex.) **(B)** Fluorescence verification of catalytic AND gate function. $[S] = 10$ nM, $[F1] = [F2] = 13$nM. $([C1], [C2]) = (2$ nM, 2 nM) is more effective at releasing output than (5 nM, 0.2 nM) and (0.2 nM, 5 nM) even though the latter combinations possess higher total catalyst concentration.

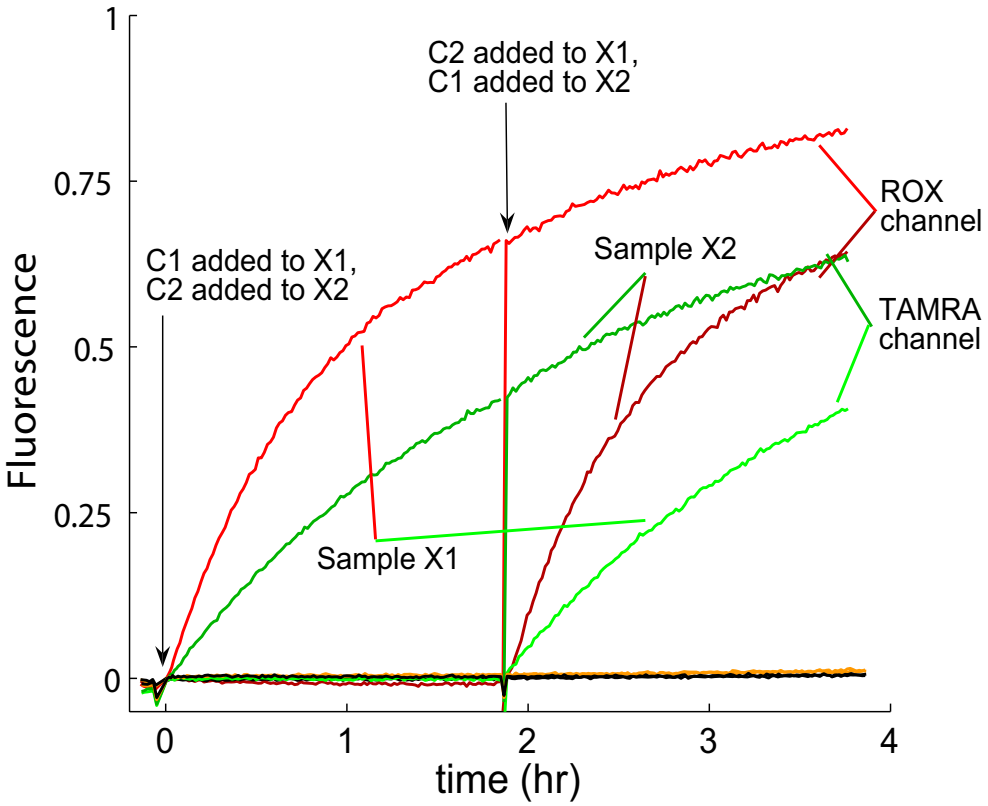

FIG. S12: Simultaneous function of two unrelated catalytic systems. The red and green traces show the same sample ($X1$), monitored in the ROX and TAMRA channel, respectively. The dark red and dark green traces show the same sample ($X2$), monitored in the ROX and TAMRA channel, respectively. Fuels for both the system presented in Fig. 1 ($F1$) and in Fig. S9 ($F2$) were present in both samples from the beginning. At $t \approx 0$, 10 nM (1x) $S1$ and $S2$ were added to both $X1$ and $X2$. Additionally, at $t \approx 0$, 0.1x $C1$ was added to $X1$, while 0.1x $C2$ was added to $X2$. Accordingly, the red and dark green traces showed increase in fluorescence due to catalytic activity, while the dark red and green traces show that catalysts $C1$ and $C2$ do not possess unwanted catalytic behavior (by catalyzing the other reaction). Control experiments showed that the ROX fluorophore in isolation is detected on the TAMRA channel with brightness 0.1112 relative to signal as detected on the ROX channel. Similarly, the TAMRA fluorophore in isolation produces signal on the ROX channel with efficiency 0.0687 relative to the signal detected on the TAMRA channel. The traces shown in this figure have been adjusted to remove fluorophore channel bleeding (using the data points between t = 0 and 1.8 hr on the red and dark green traces as references). At $t \approx 1.8$ hr, 0.1x $C1$ was added to $X2$, and 0.1x $C2$ was added to $X1$. The green and dark red traces then show increased fluorescence activity, showing that presence of other catalyst systems does not inhibit the proper function of catalysis.

[1] K. U. Mir, *Proc. DNA Based Computers II* **44**, 243 (1999).
[2] M. Zuker, *Nucleic Acids Res.* **31**, 3406 (2003).
[3] J. D. Puglisi, I. Tinoco, *Methods in Enzymology* **180**, 304 (1989).
[4] M. Torimura, S. Kurata, K. Yamada, T. Yokomaku, Y. Kamagata, T. Kanagawa, R. Kurane, *Anal. Sci.* **17**, 155 (2001).
[5] J. Santa Lucia, *Proc Natl Acad Sci USA* **95**, 1460 (1998).